J. Plasma Phys. (2023), *vol.* 89, 905890207
Published by Cambridge University Press
doi:10.1017/S0022377823000168

Generation of terahertz radiation by a Hermite–Gaussian laser beam inside magnetoplasma with a density ramp

Proxy Kad[1], **Vidisha Rana**[1] **and Arvinder Singh**[1,†]

[1]Dr. B.R. Ambedkar National Institute of Technology, Jalandhar 144011, Punjab, India

(Received 30 December 2022; revised 14 February 2023; accepted 14 February 2023)

In the present scheme of work, the Hermite–Gaussian (HG) laser beam dynamics has been investigated under the influence of an upward density ramp inside magnetized plasma, where both relativistic and ponderomotive nonlinearities are operative. One can achieve self-focusing of laser beam due to the change in the medium's dielectric function, which comes into operation due to the expulsion of plasma electrons from the high intensity to the low-intensity region by ponderomotive force and their motion at relativistic speeds. The dynamics of the laser beam and terahertz generation have been investigated by using the moment theory approach. It has been observed from the present analysis that the dynamics of the laser beam and the production of terahertz radiations strongly depends upon the HG laser beam and plasma parameters. In addition to this, the effect of density ramp and magnetic field has also been investigated on the efficiency of terahertz generation. It has been observed that higher-order modes of the HG laser beam play a dominant role in the production of terahertz radiations.

Key words: plasma nonlinear phenomena, plasma waves

1. Introduction

Terahertz radiations refer to the high-frequency radiations lying in the range of $(0.1\text{–}1)\times 10^{12}$ Hz. These radiations find a wide range of applications in the area of communication (Song & Nagatsuma 2011), spectroscopy (Beard, Turner & Schmuttenmaer 2002), medical imaging (Han 2012), security (Kemp *et al.* 2003), etc., due to their ability to penetrate any medium without causing any ionization. Terahertz generation using terawatt-level lasers was first proposed and exhibited by Hamster *et al.* (1993). Some methods to produce terahertz radiations involve using nonlinear crystals by optical rectification (Singh *et al.* 2017), photo-conduction processes (Cai *et al.* 1997) and by coupling of lasers with anharmonic carbon nanotubes (CNTs) (Kumar *et al.* 2022*a*,*b*, 2023). Using nonlinear crystals, it has been possible to go up to a laser intensity of the order of 10^{10-11} W cm^{-2}. Other methods involve using accelerator-based sources which can produce terahertz radiations with high repetition rates, brightness and power. However, the limited accessibility and availability of accelerators and the breakdown of nonlinear crystals at high-intensity electric field cause a limitation in the production of high power

† Email address for correspondence: arvinders@nitj.ac.in

and efficient terahertz radiation. An alternate way to produce efficient terahertz radiation involves using laser–plasma interaction (Hassan *et al.* 2012).

Laser–plasma interaction has led to many developments in terahertz generation (Sobhani, Dadar & Feili 2017; Sun, Wang & Zhang 2022), second-harmonic generation (Upadhyay & Tripathi 2005; Sharma, Thakur & Kant 2020), plasma-wakefield excitation for particle acceleration (Kim *et al.* 2021; Kad & Singh 2022*b*), etc. Plasma being a nonlinear medium has an extraordinarily high damage threshold, and is thus capable of sustaining a high-intensity electric field (Hassan *et al.* 2012). An electromagnetic wave can travel only small distances (called Rayleigh length) due to its tendency to diffract in any medium. But for efficient terahertz generation, the laser-medium interaction time should be long enough. Thus, using plasma as the medium, one can overcome these restrictions. The laser beam on interacting with the plasma medium undergoes nonlinear phenomena such as self-focusing (Mori *et al.* 1988), self-trapping (Singh & Walia 2010), self-compression (Saedjalil & Jafari 2016), etc. Self-focusing helps to balance out the diffraction of the laser beam in plasma by acting as a waveguide.

Much work has already been done on terahertz generation by either coupling two different laser beams (Malik, Malik & Nishida 2011) or by using a single laser beam. The efficiency of terahertz generation can be increased by introducing a density ramp, thereby taking into account the non-homogeneity of plasma. The effect of introducing a density ramp on terahertz radiation has been illustrated by Miao, Palastro & Antonsen (2016). Singh & Sharma (2013) presented terahertz generation in a rippled density plasma. Niknam *et al.* (2016) has investigated the generation of terahertz radiation in inhomogeneous collisional plasma by the interaction of two laser beams. Furthermore, the magnetic field also affects the generation of terahertz radiation by affecting the extent of self-focusing of laser beams. The effect of magnetized plasma in nonlinear plasma has been depicted by Sharma *et al.* (2010). Strong terahertz production under the non-relativistic ponderomotive regime in magnetized collisional plasma has been demonstrated by Varshney *et al.* (2018). Gupta & Jain (2021) have used a super-Gaussian laser pulse to produce terahertz radiation in magnetized plasma.

From the literature review, it has been concluded that most of the previous research work in the field of terahertz generation has been carried out by the interaction of Gaussian profile beams with a collisionless plasma medium using the paraxial theory approach. The present work demonstrates the scheme of generation of terahertz radiation using a laser beam with Hermite–Gaussian (HG) profile in magnetized plasma with a density ramp under a relativistic-ponderomotive regime. To the best of the authors' knowledge, no earlier theoretical investigation using the moment theory approach for terahertz generation has been carried out by the higher-order modes of a HG laser beam in a relativistic-ponderomotive magnetoplasma having an exponential density ramp. Ponderomotive self-focusing takes place when the electrons are expelled from the high- to low-intensity region due to the ponderomotive force which is associated with a spatial gradient in the laser beam intensity. This, along with relativistic effects, changes the refractive index and dielectric properties of the plasma medium due to the motion of plasma electrons at relativistic speeds. The paper is aimed at investigating the influence of higher-order modes of a HG laser beam, its intensity and the slope of density ramp and magnetic field on the efficiency of terahertz generation. Unlike the laser beams with Gaussian profiles which are studied by paraxial theory, its interaction with plasma is studied through the method of moments. This is because for laser beams with super-Gaussian profile such as Laguerre–Gaussian (Kad & Singh 2022*a*,2022*c*), Bessel–Gaussian (Kad *et al.* 2022), HG (Wadhwa & Singh 2020), etc., one needs to take into account the intensity of the off-axial parts along with the axial parts. In paraxial

https://doi.org/10.1017/S0022377823000168 Published online by Cambridge University Press

theory, only the axial part of the laser intensity is taken into consideration and the off-axial parts are neglected. The structure of the paper is as follows. In § 2, the HG laser beam profile is depicted. Sections 3 and 4 illustrate the modification of the dielectric function of plasma and laser dynamics inside the plasma, respectively. In § 5, plasma wave excitation and generation of terahertz radiation are discussed. The results are discussed in § 6, followed by the conclusion of the obtained results in § 7.

2. HG laser beam profile

For a laser beam propagating in plasma, the electric field vector along the z axis is given by

$$E(x, y, z) = \Psi(x, y, z)\mathrm{e}^{\mathrm{i}\{\omega t - kz\}}, \tag{2.1}$$

where, ω and k represents the angular frequency and the wavevector, respectively. Here Ψ denotes the complex amplitude of HG laser beam's electric field and the equation that governs its intensity distribution is given as

$$I = \Psi\Psi^*, \tag{2.2}$$

where

$$\Psi\Psi^* = \frac{E_{00}^2}{f_x f_y}\exp\left(-\left(\frac{x^2}{x_0^2 f_x^2} + \frac{y^2}{y_0^2 f_y^2}\right)\right) H_m^2\left(\frac{x}{x_0 f_x}\right) H_n^2\left(\frac{y}{y_0 f_y}\right). \tag{2.3}$$

Here, x_0 and y_0 denote the HG laser beam's spot size before entering the plasma along transverse axes x and y. Here E_{00} is the maximum electric field amplitude along the axis and f_x and f_y represents the beam width parameters along the transverse axes, respectively. Here m and n correspondingly depict the number of nodes along the x and y directions as well as the degrees of Hermite polynomials H_m and H_n. The intensity distribution plots for transverse electromagnetic (TEM) modes (0,0), (0,1) and (0,2) of the HG laser beam have been depicted by figures 1(*a*), 1(*b*) and 1(*c*), respectively.

3. Nonlinear dielectric function

Due to nonlinear laser–plasma interaction, a relativistic ponderomotive force acts upon the electrons in the plasma which causes a relativistic variation in its mass which implies that the rest mass of an electron (m_0) gets modified by a factor of γ (i.e. $m_0 \to m_0\gamma$). Due to this, the refractive index and the dielectric function gets modified, which now comprises of a linear (ϵ_0) and a nonlinear term $\chi(EE^*)$. Under the combined effect of magnetic field, density ramp and relativistic-ponderomotive nonlinearity, the dielectric function is obtained as follows:

$$\epsilon = \epsilon_0 + \chi(EE^*), \tag{3.1}$$

where

$$\epsilon = 1 - \frac{\omega_p^2}{\gamma\omega^2}\exp\left(-\frac{m_0 c^2}{T_e}(\gamma - 1)\right), \tag{3.2}$$

$$\epsilon_0 = 1 - \frac{\omega_p^2}{\omega^2}. \tag{3.3}$$

Where, ω_p is the non-homogeneous plasma frequency in the absence of laser beam which increases exponentially with the distance of propagation z and is given by

$$\omega_p^2 = \omega_{p0}^2 \exp\left(\frac{z/kx_0^2}{d}\right), \tag{3.4}$$

https://doi.org/10.1017/S0022377823000168 Published online by Cambridge University Press

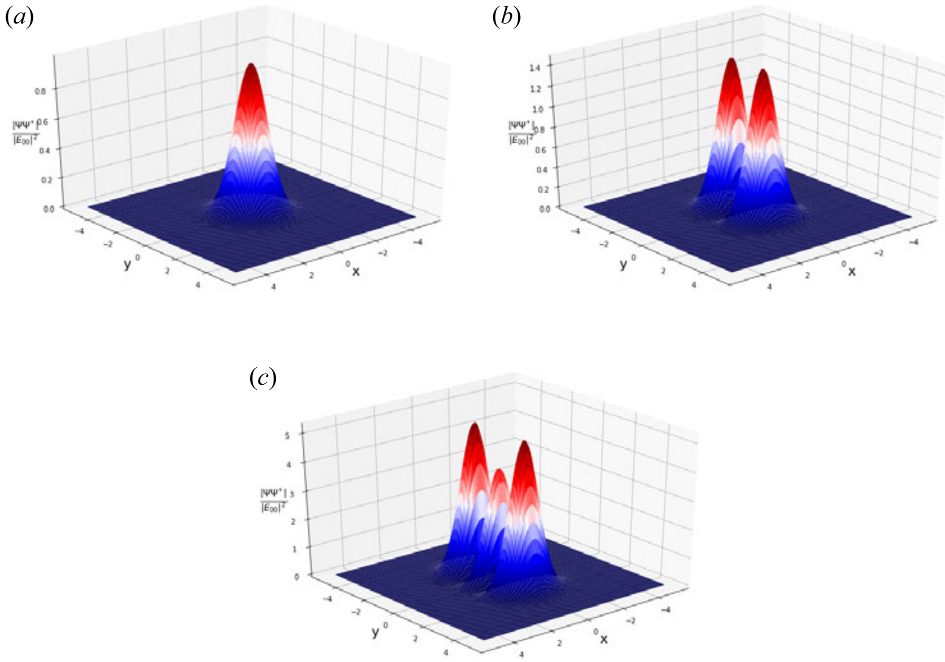

FIGURE 1. Three-dimensional normalized intensity distribution plots for various TEM modes (0,0), (0,1) and (0,2) depicted by panels (*a*), (*b*) and (*c*) respectively.

where d is the slope of density ramp, T_e is the temperature in energy units and γ is the Lorentz factor given by

$$\gamma = (1 + \beta' E E^*)^{1/2}, \tag{3.5}$$

and

$$\beta' = \frac{\beta}{\left(1 - \dfrac{\omega_c}{\omega}\right)}, \tag{3.6}$$

is the coefficient of nonlinearity which takes into account the effect of the plasma being magnetized.

Using (2.2), (3.2)–(3.5) and substituting in (3.1), the nonlinear dielectric function is obtained as

$$\chi(EE^*) = \frac{\omega_p^2}{\omega^2}\left[1 - \frac{1}{\gamma}\exp\left(\frac{-m_0 c^2}{T_e}(\gamma - 1)\right)\right]. \tag{3.7}$$

4. HG laser beam dynamics

The dynamical behaviour of the laser beam while travelling through plasma is governed by the following Maxwell's equations:

$$\nabla \times \boldsymbol{E} = -\frac{1}{c}\frac{\partial \boldsymbol{B}}{\partial t}, \tag{4.1}$$

$$\nabla \times \boldsymbol{B} = -\frac{\epsilon}{c}\frac{\partial \boldsymbol{E}}{\partial t}. \tag{4.2}$$

https://doi.org/10.1017/S0022377823000168 Published online by Cambridge University Press

On using (4.1) and (4.2) one can obtain the wave equation as

$$\nabla^2 \boldsymbol{E} - \frac{\epsilon}{c^2}\frac{\partial^2 \boldsymbol{E}}{\partial t^2} = 0. \tag{4.3}$$

Assuming that the modifications in the transverse directions are much faster than those in the z direction and using (2.1), (2.2) in (4.3), one can obtain the nonlinear Schrodinger wave equation as follows:

$$\iota \frac{\mathrm{d}\Psi}{\mathrm{d}z} = \frac{1}{4k}\left(1 + \frac{\epsilon_{0+}}{\epsilon_{0_{zz}}}\right)\nabla_\perp^2 \Psi + \frac{k}{2\epsilon_0}\chi(EE^*)\Psi. \tag{4.4}$$

Using the method of moments, given by Vlasov, Petrishchev & Talanov (1971), one can find the root mean square width of a laser beam as

$$a_{rms} = \frac{\int_{-\infty}^{\infty}\int_{-\infty}^{\infty}(x^2+y^2)\Psi\Psi^*\,\mathrm{d}x\,\mathrm{d}y}{\int_{-\infty}^{\infty}\int_{-\infty}^{\infty}\Psi\Psi^*\,\mathrm{d}x\,\mathrm{d}y}. \tag{4.5}$$

On differentiating equation (4.5) twice with respect to z and using (4.4), we get

$$\frac{\mathrm{d}^2 a_{rms}}{\mathrm{d}z^2} = \frac{2}{k\int_{-\infty}^{\infty}\int_{-\infty}^{\infty}\Psi\Psi^*\,\mathrm{d}x\,\mathrm{d}y}\left\{\frac{1}{4k}\left(1+\frac{\epsilon_{0+}}{\epsilon_{0zz}}\right)^2\int_{-\infty}^{\infty}\int_{-\infty}^{\infty}|\nabla_\perp\Psi|^2\,\mathrm{d}x\,\mathrm{d}y \right.$$
$$\left. + \frac{k}{4\epsilon_0}\left(1+\frac{\epsilon_{0+}}{\epsilon_{0zz}}\right)\int_{-\infty}^{\infty}\int_{-\infty}^{\infty}|\Psi|^2\left(x\frac{\partial\chi(EE^*)}{\partial x} + y\frac{\partial\chi(EE^*)}{\partial y}\right)\mathrm{d}x\,\mathrm{d}y\right\}. \tag{4.6}$$

On using (2.2) in (4.5), we obtain the value of a_{rms} as

$$a_{rms} = x_0^2 f_x^2\left(m+\frac{1}{2}\right) + y_0^2 f_y^2\left(n+\frac{1}{2}\right). \tag{4.7}$$

On differentiating equation (4.7) with respect to z and using (2.2), (3.7) and (4.6), we get the two coupled second-order differential equations as

$$\frac{\mathrm{d}^2 f_x}{\mathrm{d}\zeta^2} + \frac{1}{f_x}\left(\frac{\mathrm{d}f_x}{\mathrm{d}\zeta}\right)^2 = \frac{1}{4}\left(1+\frac{\epsilon_{0+}}{\epsilon_{0zz}}\right)^2\frac{1}{f_x^3} + \frac{1}{2}\left(1+\frac{\epsilon_{0+}}{\epsilon_{0zz}}\right)\frac{\beta' E_{00}^2}{\pi f_x^2 f_y}\Phi$$
$$\frac{I_1}{\left(1-\dfrac{\omega_c}{\omega}\right)(m+1/2)2^{m+n+1}m!n!}, \tag{4.8}$$

$$\frac{\mathrm{d}^2 f_y}{\mathrm{d}\zeta^2} + \frac{1}{f_y}\left(\frac{\mathrm{d}f_y}{\mathrm{d}\zeta}\right)^2 = \frac{1}{4}\left(1+\frac{\epsilon_{0+}}{\epsilon_{0zz}}\right)^2\frac{(x_0/y_0)^4}{f_y^3} + (x_0/y_0)^4\frac{1}{2}\left(1+\frac{\epsilon_{0+}}{\epsilon_{0zz}}\right)\frac{\beta' E_{00}^2}{\pi f_x f_y^2}$$
$$\Phi\frac{I_2}{\left(1-\dfrac{\omega_c}{\omega}\right)(n+1/2)2^{m+n+1}m!n!}, \tag{4.9}$$

https://doi.org/10.1017/S0022377823000168 Published online by Cambridge University Press

where

$$I_1 = \int_{-\infty}^{\infty}\int_{-\infty}^{\infty} x' \exp\left(-2\left(x'^2 + y'^2 + \frac{m_0c^2(J(x', y')^{1/2} - 1)}{2T_e}\right)\right)$$
$$\times H_m^3(x')H_n^4(y')\frac{(x'H_m(x') - H_{m+1}(x'))}{J(x', y')}\left(\frac{1}{J(x', y')^{1/2}} - \frac{m_0c^2}{T_e}\right) \mathrm{d}x'\,\mathrm{d}y', \tag{4.10}$$

$$I_2 = \int_{-\infty}^{\infty}\int_{-\infty}^{\infty} y' \exp\left(-2\left(x'^2 + y'^2 + \frac{m_0c^2(J^{1/2} - 1)}{2T_e}\right)\right)$$
$$\times H_m^4(x')H_n^3(y')\frac{(y'H_n(y') - H_{n+1}(y'))}{J(x', y')}\left(\frac{1}{J(x', y')^{1/2}} - \frac{m_0c^2}{T_e}\right) \mathrm{d}x'\,\mathrm{d}y', \tag{4.11}$$

and where

$$J(x', y') = \left(1 + \frac{\beta'\psi_{00}^2}{f_xf_y}H_m^2(x')H_n^2(y')\exp(-(x'^2 + y'^2))\right), \tag{4.12}$$

$$\varPhi = \left(\frac{\omega_{p0}^2{x_0}^2}{c^2}\right)\exp\left(\frac{\zeta}{d}\right), \tag{4.13}$$

$$x' = \frac{x}{x_0f_x}, \tag{4.14}$$

$$y' = \frac{y}{y_0f_y}, \tag{4.15}$$

$$\zeta = \frac{z}{kx_0^2} \tag{4.16}$$

is the dimensionless distance of propagation.

On solving (4.8) and (4.9) numerically and subjecting them to boundary conditions $f_{x,y} = 1$ and $f'_{x,y} = 0$ dictates the spot size variation of HG laser beam along the transverse x and y directions, respectively.

5. Electron plasma wave excitation and terahertz generation

Poisson's equation, the adiabatic equation of state, the equation of motion and the continuity equation are the four main equations that govern the excitation of the electron plasma wave. The relativistic-ponderomotive force experienced by the electrons is given by

$$F_{R-P} = -m_0c^2\nabla(\gamma - 1), \tag{5.1}$$

and following Wadhwa & Singh (2020), the expression for perturbed electron density is given as

$$n_1 = -\frac{en_0}{m_0}\frac{E_{00}}{\sqrt{f_xf_y}}\exp\left(-\left(\frac{x^2}{x_0^2f_x^2} + \frac{y^2}{y_0^2f_y^2}\right)\right)\left\{H_m\left(\frac{x}{x_0f_x}\right)H_n\left(\frac{y}{y_0f_y}\right)\left(\frac{x}{x_0^2f_x^2} + \frac{y}{y_0^2f_y^2}\right)\right.$$
$$\left. - \frac{1}{x_0f_x}H_{m+1}\left(\frac{x}{x_0f_x}\right)H_n\left(\frac{y}{y_0f_y}\right) - \frac{1}{y_0f_y}H_m\left(\frac{x}{x_0f_x}\right)H_{n+1}\left(\frac{y}{y_0f_y}\right)\right\}$$
$$\frac{1}{\left(\omega^2 - k^2v_T^2 - \frac{\omega_p^2}{\gamma}\exp\left(\frac{-m_0c^2}{T_e}(\gamma - 1)\right)\right)}. \tag{5.2}$$

https://doi.org/10.1017/S0022377823000168 Published online by Cambridge University Press

The wave equation governing terahertz generation is given as

$$\nabla^2 E_{Th} + \frac{\omega_{Th}^2}{c^2}\epsilon_{Th}(\omega_{Th})E_{Th} = \frac{\omega_p^2}{c^2}\left(\frac{n_1}{n_0}\right)E, \tag{5.3}$$

where, ϵ_{Th} $(= k_{Th}^2 c^2/\omega_{Th}^2)$ is the dielectric constant at terahertz frequency and $\omega_{Th} = \omega - \omega_{ep}$ is the terahertz radiation frequency. Taking $E_{Th} = A_{Th}\exp(\mathrm{i}(w_{Th}t - k_{Th}z))$ where A_{Th} is the amplitude of the generated terahertz radiation and considering that the change in the z direction is much greater than in the transverse directions (i.e. $\partial E_{Th}/\partial z > \partial E_{Th}/\partial r$), (5.3) can be written as

$$2\mathrm{i}k_{Th}\frac{\partial A_{Th}}{\partial z} \approx \frac{\omega_p^2}{c^2}\frac{n_1}{n_0}\Psi, \tag{5.4}$$

where the magnitude of wavevector of terahertz generation is

$$k_{Th} = \frac{\omega}{c}\left(1 - \frac{\omega_p^2}{\omega^2}\right)^{1/2}. \tag{5.5}$$

The yield η of terahertz radiation is evaluated as

$$\eta = \frac{P_{Th}}{P_0}, \tag{5.6}$$

where, P_{Th} is the power of the generated terahertz radiation and P_0 is the power of incident laser beam. Since power is directly proportional to the intensity, it can be calculated (Sodha, Ghatak & Tripathi 1976) as

$$P_{Th} = \frac{c}{8\pi}\int_{-\infty}^{\infty}\int_{-\infty}^{\infty} A_{Th}A_{Th}^*\,\mathrm{d}x\,\mathrm{d}y, \tag{5.7}$$

$$P_0 = \frac{c}{8\pi}\int_{-\infty}^{\infty}\int_{-\infty}^{\infty} \Psi\Psi^*\,\mathrm{d}x\,\mathrm{d}y. \tag{5.8}$$

Using (5.7) and (5.8) in (5.6), we get

$$\eta = \frac{\beta' E_{00}^2}{f_x f_y}\Phi\frac{I_3}{2^{m+n}\pi m!n!}, \tag{5.9}$$

where,

$$I_3 = \int_{-\infty}^{\infty}\int_{-\infty}^{\infty}\exp(-2(x'^2 + y'^2))H_m^2(x')H_n^2(y')\left(H_m(x')H_n(y')\left(\frac{x'}{f_x} + \frac{x_0}{y_0}\frac{y'}{f_y}\right)\right.$$
$$\left. - \frac{1}{f_x}H_{m+1}(x')H_n(y') - \frac{x_0}{y_0 f_y}H_m(x')H_{n+1}(y')\right)^2$$
$$\frac{1}{\left(\dfrac{\omega^2 x_0^2}{c^2} - \left(\dfrac{\omega^2 x_0^2}{c^2} - \Phi\right)\dfrac{v_T^2}{c^2} - \dfrac{\Phi}{\gamma}\left(\dfrac{-m_0 c^2}{T_e}(\gamma - 1)\right)\right)^2}\,\mathrm{d}x'\,\mathrm{d}y'. \tag{5.10}$$

https://doi.org/10.1017/S0022377823000168 Published online by Cambridge University Press

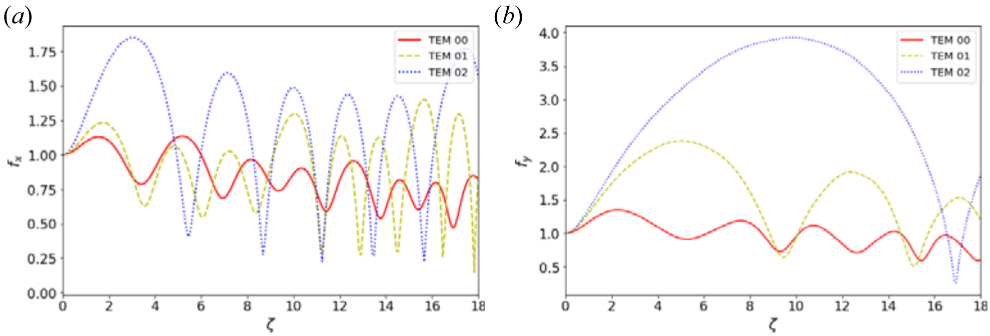

FIGURE 2. Change in f_x and f_y with ζ for higher-order modes at specified values of $d = 10$, normalized plasma density $\omega_{p0}^2 x_0^2/c^2 = 12$, $\omega_c = 0.1\omega$, normalized laser intensity $\beta\psi_{00}^2 = 2$, $T_e = 10$ KeV and $x_0/y_0 = 1$ as depicted by panels (*a*) and (*b*), respectively.

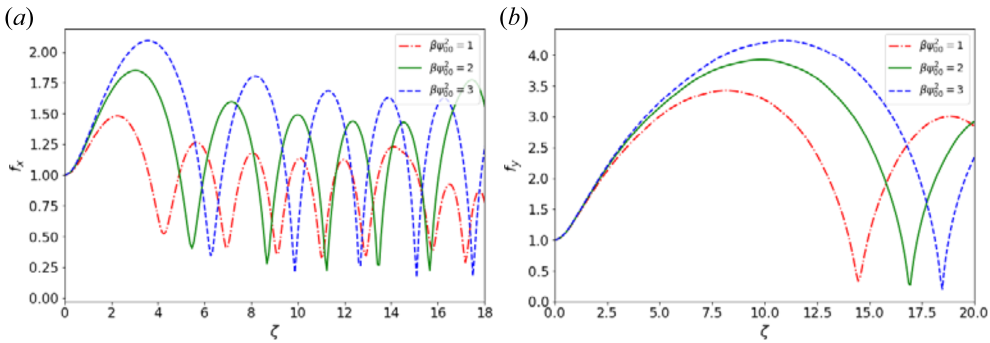

FIGURE 3. Change in f_x and f_y with ζ for various normalized intensities at specified values of $d = 10$, TEM mode $(m, n) = (0, 2)$, $\omega_c = 0.1\omega$, normalized plasma density $\omega_{p0}^2 x_0^2/c^2 = 12$, $T_e = 10$ KeV and $x_0/y_0 = 1$ as depicted by panels (*a*) and (*b*), respectively.

6. Results and discussion

Self-focusing of the HG laser beam and the variation of the beam width variables f_x and f_y with the dimensionless distance of propagation ζ under the effect of magnetic field and upward density ramp has been analysed by solving (4.8) and (4.9) simultaneously. Also, the effect of different parameters such as density ramp slope, static magnetic field, etc., on the efficiency of terahertz generation has been studied. Simulation of the mentioned work has been carried out using the following set of laser variables: $\omega = 1.78 \times 10^{15}$ rad s^{-1} (Nd: YAG laser beam) and $x_0 = 15$ µm.

Figure 2(*a*,*b*) represent the change in f_x and f_y for different modes with respect to ζ at a fixed value of 'd' $= 10$ and $\omega_c = 0.1\omega$. These depict the oscillatory nature of f_x and f_y which correspond to the beam's convergence and divergence while propagating inside the plasma. The application of a magnetic field enhances self-focusing in both transverse directions. Due to the coupling of f_x and f_y, maximum focusing is achieved for the TEM$_{02}$ mode as compared with TEM$_{00}$ and TEM$_{01}$. This is due to the symmetric distribution of intensity along the y axis as depicted in figure 1(*c*) with the intensity being maximum in the off-axial parts. Also, due to the presence of a density ramp, the self-focusing of the laser beam increases with ζ as the diffraction effects are minimized. This is because the

https://doi.org/10.1017/S0022377823000168 Published online by Cambridge University Press

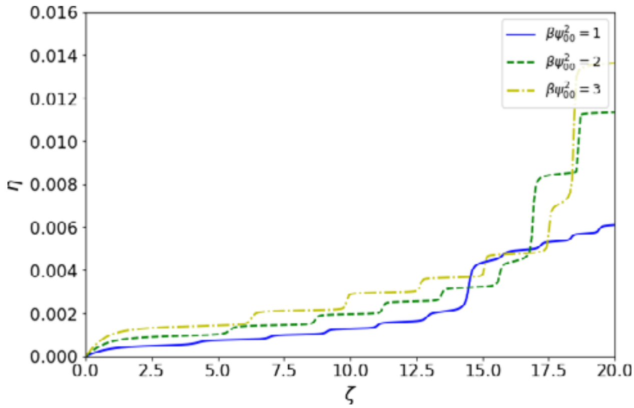

FIGURE 4. Modification in efficiency η of generated terahertz radiation with ζ for various normalized intensities at specified values of $d = 10$, TEM mode $(m, n) = (0, 2)$, $\omega_c = 0.1\omega$, normalized plasma density $\omega_{p0}^2 x_0^2/c^2 = 12$, $T_e = 10$ KeV and $x_0/y_0 = 1$.

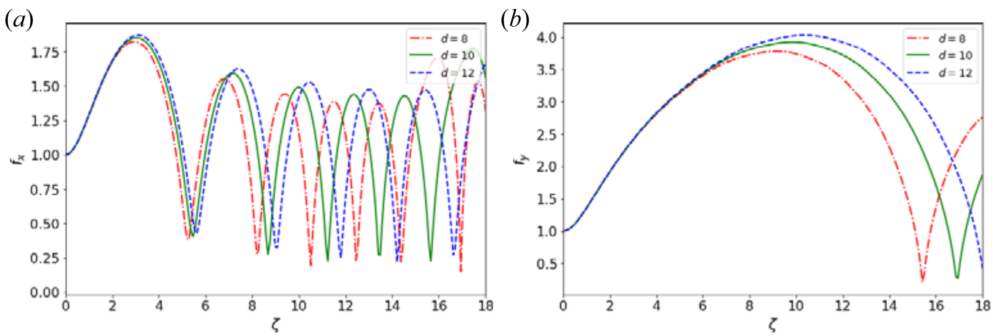

FIGURE 5. Change in f_x and f_y with ζ for various values of d at specified values of normalized laser intensity $\beta\psi_{00}^2 = 2$, TEM mode $(m, n) = (0, 2)$, $\omega_c = 0.1\omega$, normalized plasma density $\omega_{p0}^2 x_0^2/c^2 = 12$, $T_e = 10$ KeV and $x_0/y_0 = 1$ as depicted by panels (*a*) and (*b*), respectively.

density ramp profile acts as a slowly narrowing waveguide for the laser beam propagating inside the plasma. The increase in laser intensity leads to an increase in the nonlinearity of the medium, which then results in a high refractive index and thus better focusing in the transverse directions as shown by figure 3(*a*,*b*). This increase in self-focusing leads to an increase in the efficiency of generated terahertz radiation (figure 4).

Figure 5(*a*,*b*) illustrate the effect of the slope of density ramp '*d*' on the focusing of the laser beam. It is observed from the figures that there is more self-focusing as the value of '*d*' decreases. This is due to the dominance of the nonlinear refractive term over the diffractive term as the value of '*d*' decreases. As the value of '*d*' increases, the density variation/transition goes on decreasing (figure 5*a*,*b*). Therefore, the efficiency of generated terahertz radiation also increases with a decrease in the value of '*d*' (figure 6). Figure 7(*a*,*b*) show that the increase in the applied magnetic field results in deeper self-focusing and hence greater efficiency (η) of terahertz radiation (figure 8). Figure 8 depicts the efficiency variation with ζ at different values of $\omega_c = 0.1, 0.2$ and 0.3. An

https://doi.org/10.1017/S0022377823000168 Published online by Cambridge University Press

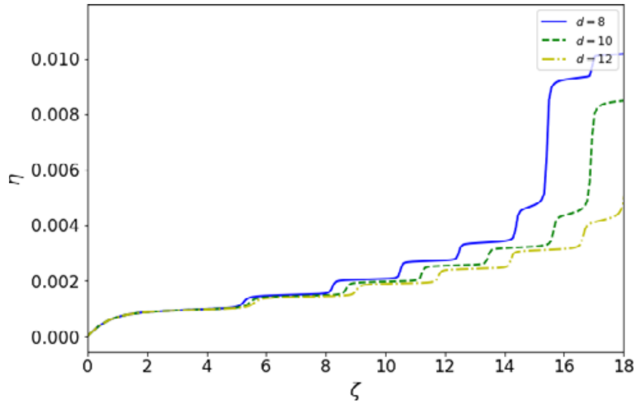

FIGURE 6. Modification in efficiency η of generated terahertz radiation with ζ for various d at specified values of normalized laser intensity $\beta\psi_{00}^2 = 2$, TEM mode $(m, n) = (0, 2)$, $\omega_c = 0.1\omega$, normalized plasma density $\omega_{p0}^2 x_0^2/c^2 = 12$, $T_e = 10$ KeV and $x_0/y_0 = 1$.

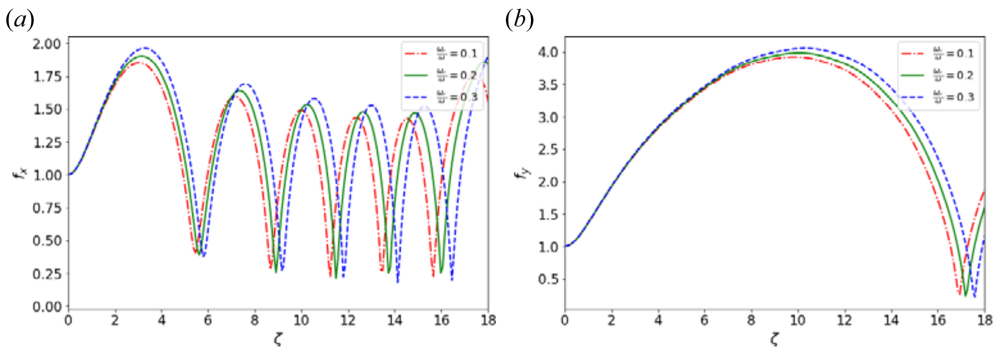

FIGURE 7. Change in f_x and f_y with ζ for various values of ω_c at specified values of normalized laser intensity $\beta\psi_{00}^2 = 2$, TEM mode $(m, n) = (0, 2)$, $d = 10$, normalized plasma density $\omega_{p0}^2 x_0^2/c^2 = 12$, $T_e = 10$ KeV and $x_0/y_0 = 1$ as depicted by panels (*a*) and (*b*), respectively.

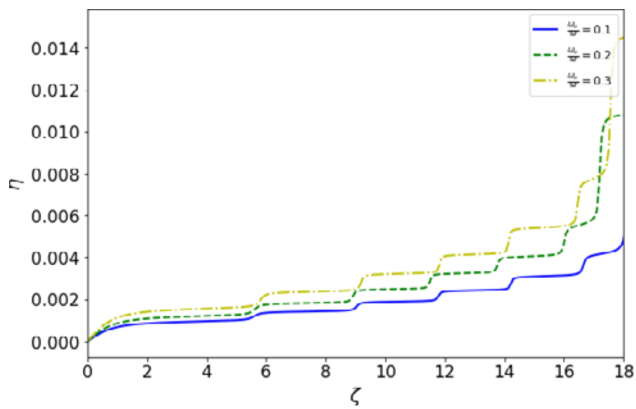

FIGURE 8. Modification in efficiency η of generated terahertz radiation with ζ for various ω_c at specified values of $d = 10$, normalized laser intensity $\beta\psi_{00}^2 = 2$, TEM mode $(m, n) = (0, 2)$, normalized plasma density $\omega_{p0}^2 x_0^2/c^2 = 12$, $T_e = 10$ KeV and $x_0/y_0 = 1$.

https://doi.org/10.1017/S0022377823000168 Published online by Cambridge University Press

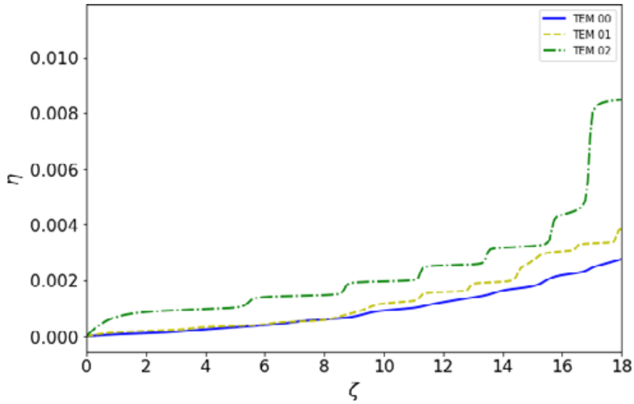

FIGURE 9. Modification in efficiency η of generated terahertz radiation with ζ for various higher-order modes at specified values of $d = 10$, normalized plasma density $\omega_{p0}^2 x_0^2/c^2 = 12$, $\omega_c = 0.1\omega$, normalized laser intensity $\beta\psi_{00}^2 = 2$, $T_e = 10\,\mathrm{KeV}$ and $x_0/y_0 = 1$.

increase in the value of the magnetic field leads to more convergence and hence more efficiency.

Figure 9 represents efficiency variation of generated terahertz radiation with ζ for different TEM modes. Efficiency is better for TEM_{02} as compared with TEM_{00} and TEM_{01} because of its better self-focusing as compared with other modes.

7. Conclusions

The present work demonstrates the HG laser beam dynamics and terahertz generation while propagating through plasma under the effect of an exponential density ramp and a static magnetic field in a relativistic-ponderomotive regime. It has been observed that self-focusing is more for TEM_{02} as compared with other modes and it also increases with an increase in normalized laser intensity, applied magnetic field and with a decrease in the slope of density ramp 'd'. It is concluded from the present investigation that maximum terahertz efficiency is observed for TEM_{02} and further efficiency is also enhanced at higher values of normalized laser intensity, applied magnetic field and with a decrease in the density ramp slope. The results of the present investigation may be useful for the experimentalist working in the field of terahertz generation.

Acknowledgements

Editor V. Malka thanks the referees for their advice in evaluating this article.

Funding

The authors express their gratitude towards the Ministry of Education, India, for providing financial support to carry out this research work.

Declaration of interests

The authors report no conflict of interest.

REFERENCES

BEARD, M.C., TURNER, G.M. & SCHMUTTENMAER, C.A. 2002 Terahertz spectroscopy. *J. Phys. Chem. B* **106** (29), 7146–7159.

https://doi.org/10.1017/S0022377823000168 Published online by Cambridge University Press

CAI, Y., BRENER, I., LOPATA, J., WYNN, J., PFEIFFER, L. & FEDERICI, J. 1997 Design and performance of singular electric field terahertz photoconducting antennas. *Appl. Phys. Lett.* **71** (15), 2076–2078.

GUPTA, D.N. & JAIN, A. 2021 Terahertz radiation generation by a super-Gaussian laser pulse in a magnetized plasma. *Optik* **227**, 165824.

HAMSTER, H., SULLIVAN, A., GORDON, S., WHITE, W. & FALCONE, R.W. 1993 Subpicosecond, electromagnetic pulses from intense laser-plasma interaction. *Phys. Rev. Lett.* **71** (17), 2725.

HAN J.K. 2012 Terahertz medical imaging. In *Convergence of Terahertz Sciences in Biomedical Systems* (eds. G.S. Park, Y.H. Kim, H. Han, J.K. Han, J. Ahn, J.H. Son, W.Y. Park & Y.U. Jeong), pp. 351–371. Springer.

HASSAN, M.B., AL-JANABI, A.H., SINGH, M. & SHARMA, R.P. 2012 Terahertz generation by the high intense laser beam. *J. Plasma Phys.* **78** (5), 553–558.

KAD, P., CHOUDHARY, R., BHATIA, A., WALIA, K. & SINGH, A. 2022 Study of two cross focused Bessel–Gaussian laser beams on electron acceleration in relativistic regime. *Optik* **271**, 170117.

KAD, P. & SINGH, A. 2022*a* Coupled effect of spatio-temporal variation of Laguerre–Gaussian laser pulse on electron acceleration in magneto-plasma. *Waves Random Complex Media*, 1–19.

KAD, P. & SINGH, A. 2022*b* Electron acceleration and spatio-temporal variation of Laguerre–Gaussian laser pulse in relativistic plasma. *Eur. Phys. J. Plus* **137** (8), 1–13.

KAD, P. & SINGH, A. 2022*c* Spatio-temporal variation of Laguerre Gaussian laser pulse and its effect on electron acceleration. *Chin. J. Phys* **82**, 171–181.

KEMP, M.C., TADAY, P.F., COLE, B.E., CLUFF, J.A., FITZGERALD, A.J. & TRIBE, W.R. 2003 Security applications of terahertz technology. In *Terahertz for Military and Security Applications* (eds. R.J. Hwu & D.L. Woolard), vol. 5070, pp. 44–52.

KIM, H.T., PATHAK, V.B., HOJBOTA, C.I., MIRZAIE, M., PAE, K.H., KIM, C.M., YOON, J.W., SUNG, J.H. & LEE, S.K. 2021 Multi-GeV laser wakefield electron acceleration with PW lasers. *Appl. Sci.* **11** (13), 5831.

KUMAR, S., VIJ, S., KANT, N. & THAKUR, V. 2022*a* Resonant excitation of THz radiations by the interaction of amplitude-modulated laser beams with an anharmonic CNTs in the presence of static dc electric and magnetic fields. *Chin. J. Phys.* **78**, 453–462.

KUMAR, S., VIJ, S., KANT, N. & THAKUR, V. 2022*b* Resonant terahertz generation by cross-focusing of Gaussian laser beams in the array of vertically aligned anharmonic and magnetized CNTs. *Opt. Commun.* **513**, 128112.

KUMAR, S., VIJ, S., KANT, N. & THAKUR, V. 2023 Nonlinear interaction of amplitude-modulated gaussian laser beam with anharmonic magnetized and rippled CNTs: THz generation. *Braz. J. Phys.* **53** (2), 37.

MALIK, A.K., MALIK, H.K. & NISHIDA, Y. 2011 Terahertz radiation generation by beating of two spatial-Gaussian lasers. *Phys. Lett.* A **375** (8), 1191–1194.

MIAO, C., PALASTRO, J.P. & ANTONSEN, T.M. 2016 Laser pulse driven terahertz generation via resonant transition radiation in inhomogeneous plasmas. *Phys. Plasmas* **23** (6), 063103.

MORI, W.B., JOSHI, C., DAWSON, J.M., FORSLUND, D.W. & KINDEL, J.M. 1988 Evolution of self-focusing of intense electromagnetic waves in plasma. *Phys. Rev. Lett.* **60** (13), 1298.

NIKNAM, A.R., BANJAFAR, M.R., JAHANGIRI, F., BARZEGAR, S. & MASSUDI, R. 2016 Resonant terahertz radiation from warm collisional inhomogeneous plasma irradiated by two Gaussian laser beams. *Phys. Plasmas* **23** (5), 053110.

SAEDJALIL, N. & JAFARI, S. 2016 Self-focusing and self-compression of a laser pulse in the presence of an external tapered magnetized density-ramp plasma. *High Energy Density Phys.* **19**, 48–57.

SHARMA, R.P., MONIKA, A., SHARMA, P., CHAUHAN, P. & JI, A. 2010 Interaction of high power laser beam with magnetized plasma and THz generation. *Laser Part. Beams* **28** (4), 531–537.

SHARMA, V., THAKUR, V. & KANT, N. 2020 Second harmonic generation of cosh-gaussian laser beam in magnetized plasma. *Opt. Quant. Electron.* **52** (10), 1–9.

SINGH, A. & WALIA, K. 2010 Relativistic self-focusing and self-channeling of gaussian laser beam in plasma. *Appl. Phys.* B **101** (3), 617–622.

SINGH, M. & SHARMA, R.P. 2013 THz generation by cross-focusing of two laser beams in a rippled density plasma. *Europhys. Lett.* **101** (2), 25001.

SINGH, R.K., SINGH, M., RAJOURIA, S.K. & SHARMA, R.P. 2017 High power terahertz radiation generation by optical rectification of a shaped pulse laser in axially magnetized plasma. *Phys. Plasmas* **24** (10), 103103.

SOBHANI, H., DADAR, E. & FEILI, S. 2017 Effective factors on twisted terahertz radiation generation in a rippled plasma. *J. Plasma Phys*. **83** (1), 655830101.

SODHA, M.S., GHATAK, A.K. & TRIPATHI, V.K. 1976 V self focusing of laser beams in plasmas and semiconductors. In *Progress in Optics* (ed. E. Wolf), vol. 13, pp. 169–265. Elsevier.

SONG, H.J. & NAGATSUMA, T. 2011 Present and future of terahertz communications. *IEEE Trans. Terahertz Sci. Technol*. **1** (1), 256–263.

SUN, W., WANG, X. & ZHANG, Y. 2022 Terahertz generation from laser-induced plasma. *Opt. Electron. Sci*. **1** (8), 220003.

UPADHYAY, A. & TRIPATHI, V.K. 2005 Second harmonic generation in a laser channel. *J. Plasma Phys*. **71** (3), 359–366.

VARSHNEY, P., UPADHAYAY, A., MADHUBABU, K., SAJAL, V. & CHAKERA, J.A. 2018 Strong terahertz radiation generation by cosh-gaussian laser beams in axially magnetized collisional plasma under non-relativistic ponderomotive regime. *Laser Part. Beams* **36** (2), 236–245.

VLASOV, S.N., PETRISHCHEV, V.A. & TALANOV, V.I. 1971 Averaged description of wave beams in linear and nonlinear media (the method of moments). *Radiophys. Quant. Electron*. **14** (9), 1062–1070.

WADHWA, J. & SINGH, A. 2020 Enhanced second harmonic generation of Hermite–Gaussian laser beam in plasma having density transition. *Laser Phys*. **30** (4), 046001.